International Conference on Space Optics—ICSO 2022

Dubrovnik, Croatia

3–7 October 2022

Edited by Kyriaki Minoglou, Nikos Karafolas, and Bruno Cugny,

The LSTM instrument: design, technology and performance

The LSTM instrument: design, technology and performance

François Bernard[a], Guillaume Bourgeois[b], Ilias Manolis[a], Itziar Barat[a], Ana Bolea Alamañac[a], Miguel Such Taboada[a], Pilar Mingorance[a], Alessandra Ciapponi[a], Tiziana Cardone[a], Etienne Dutruel[a], Gianluca Furano[a], Adrian Garcia[a], Pascal Hallibert[a], Arvid Hammar[a], David Merodio Codinachs[a], Sandro Patti[a], Piotr Skrzypek[a], Thierry Tirolien[a], Vincent Chorvalli[b], Sophie De Zotti[b], Emilie Steck[b], Nicolas Guardiola[b], Pierre-Olivier Antoine[b], Jean-Christophe Nonnet[b], Michael Seymour[b], Olivier Gry[b], Paul Jougla[b], Oriol Alvarez Trotta[c], and Isabel Cabeza Vega[c]

[a]European Space Agency - ESTEC, Keplerlaan 1, PO box 299, 2200AG Noordwijk, The Netherlands
[b]Airbus Defence and Space, Rue des Cosmonautes 31, 31402 Toulouse, France
[c]Airbus Defence and Space, Avenida de Aragón 404, 28022 Madrid, Spain

ABSTRACT

The Land Surface Temperature Monitoring (LSTM), part of the expansion missions of the Copernicus programme, aims at providing data for land surface temperature and evapotranspiration at unprecedented spatio-temporal resolution, with the main objective of providing valuable data for improved water management at individual European field scale. This paper gives an overview of the instrument main requirements flowing down from the mission objectives, and the instrument design selected to fulfill them. The technical challenges are described as well as the preliminary predicted performances.

Keywords: Copernicus, Earth observation, thermal infrared, multi-spectral imager, Land Surface Temperature

1. INTRODUCTION

1.1 Mission context and requirements

The "High Spatio-Temporal Resolution Land Surface Temperature Monitoring (LSTM) Mission" has been identified as one of the Copernicus Expansion Missions with the overall objective to complement Sentinel observation capabilities with unprecedented spatio-temporal resolution Thermal Infrared (TIR) observations over land and coastal regions in support of agriculture management services, and a range of additional services. The mission is designed to provide measurements of land surface temperature (LST) and emissivity (LSE)[1] in response to presently unfulfilled user requirements related to agricultural monitoring, with the primary objective to monitor evapotranspiration (ET) rate at European field scale by allowing more robust estimates of field-scale water productivity. The mapping and monitoring of a range of additional services benefiting from TIR observations such as soil composition, urban heat islands, coastal zone management and High-Temperature Events (HTE) is added as a complementary objective, not driving the mission design and performance. The user-required accuracy of ET retrieval (15% systematic error and 5% random error) translates into an LST measurement accuracy of 1K to 1.5K while the defined 1 ha field-scale imposes a spatial sampling of 50 m. A global geometrical revisit time of 2 days at Equator is achieved with 2 identical LSTM satellites, phased at 180° leading to almost daily revisit over Europe. The TIR observations need to be co-located with observations in visible (VIS), near infrared (NIR) and short wave infrared (SWIR) bands at equal or higher spatial sampling for the estimation of water vapor content, cloud detection and accurate geolocation.[2] A maximum latency of 6h to 12h on the LST data (Level 2), allowing for a timely delivery of ET data (Level 3) to the users 9h to 18h after observation, imposes that all Level 1 processing, such as radiometric calibration, correction, re-sampling and geolocation are performed in 3h to 6h. The development of the LSTM mission has been awarded by the European Space Agency (ESA) to an industrial consortium led by Airbus Defense and Space - Spain (Madrid), with the payload development placed under the responsibility of Airbus Defence and Space - France (Toulouse). The LSTM mission will be the

last to launch (2029) in a series of other institutional missions such as ECOSTRESS (NASA) on board the ISS, SBG (Surface Biology and Geology from NASA, mid-2020s) or TRISHNA (CNES-ISRO, 2025). The latter two missions combined with LSTM will allow for a continuous set of thermal data from the middle of this decade until the end of the LSTM operational life (no earlier than 2038).

1.2 Space segment and observation scheme

Each satellite (Figure 1) will be operated at an average altitude of 651 km in Sun Synchronous Orbit, allowing for observations over Europe at a Mean Local Solar Time (MLST), descending, of 13:00. Observations in TIR are planned during night and daytime whereas VNIR and SWIR observations are only performed during daytime. Each satellite embarks a single multi-spectral whiskbroom radio-imager covering eleven spectral bands spread within three focal planes. The ground projection of each focal plane and scanning pattern are shown on Figure 2.
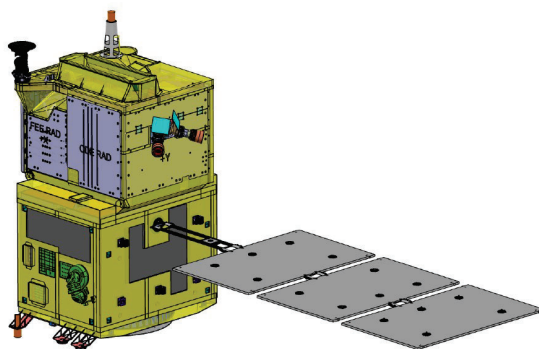
Figure 1. General view of the LSTM satellite. The payload composes the upper module on this picture
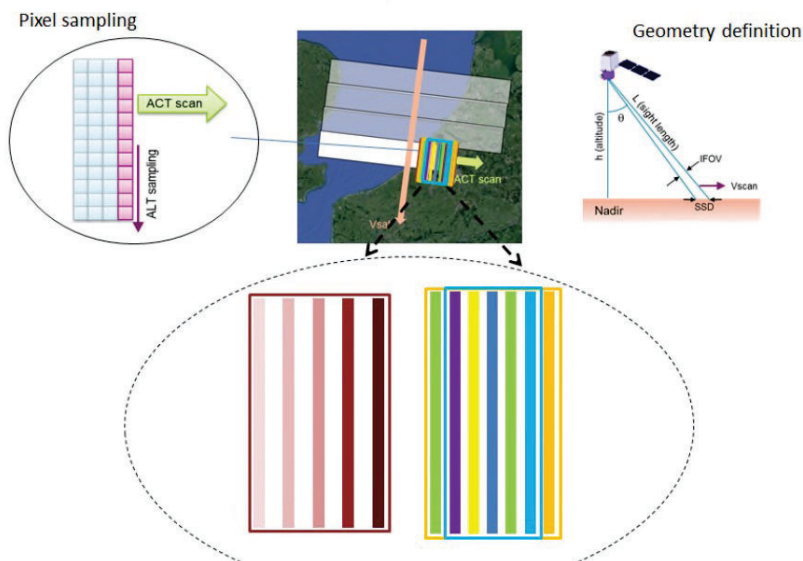
Figure 2. LSTM scanning pattern

2. THE LSTM INSTRUMENT

2.1 Key requirements

The LSTM mission objectives have been translated into a set of requirements applicable to the payload, presented in Table 1 and Table 2 for the VNIR-SWIR bands (also referred to as solar channels) and TIR bands respectively. The performance imposed to the instrument can be categorized into spectral, radiometric and image quality requirements.

The spectral bands to be acquired are defined by their central wavelength and spectral width, on which stringent tolerance (between 1.5nm and 10nm depending on the bands in VNIR-SWIR, $\leq$ 20nm in TIR) and knowledge (0.2nm to 1nm in VNIR-SWIR and $\leq$ 5nm in TIR) are demanded. Knowledge is a prime importance as it influences directly the end-product quality. The Instrument Spectral Response Function (ISRF) is indeed used in the LST retrieval algorithms. The shape of the ISRF is strictly controlled in order to guarantee very good rejection ratio of the integrated incoming signal which lies out of the spectral band of interest, compared to the in-band signal.

In the thermal bands, for the sake of simplicity in the interpretation of the requirements, all radiometric performances are expressed in terms of brightness temperature, and the dynamic range is defined, in agreement with the mission objectives, between 250 K and 460 K. For the Sun channels, a set of radiance spectra, similar to the ones specified on Sentinel-2 mission, defines the useful signal dynamic range. The signal-to-noise ratio (SNR) (resp. Noise Equivalent delta Temperature or NEdT), translates the need for radiometric precision, *i.e.* the dispersion of the recorded radiance (resp. brightness temperature) due to measurement noise.

The Absolute Radiometric Accuracy (ARA) quantifies the systematic measurement deviation from its "true" value while the Relative Spectral (resp. spatial) Radiometric Accuracy, RSRA (resp. RXRA) ensures that the systematic radiometric error remains similar from one spectral band (resp. one spatial sample) to the other. Additionally a pseudo-noise requirement has been introduced to account for the radiometric error introduced by the instrument PSF, through the unavoidable contribution of optical diffraction or by the Line of Sight (LoS) instabilities.[3]

The spatial resolution, *i.e.* the ability of the instrument to spatially resolve object on-ground, is specified through the Modulation Transfer Function at Nyquist frequency (*a.k.a.* the sampling frequency). Because of the Earth ellipsoid shape, the native sampling frequency of LSTM is not constant over the swath inducing an across-swath varying sampling frequency. The MTF is specified on the L1b product, at a ground-projected frequency equivalent to 50m sampling grid.

This set of demanding requirements brings several constraints on the design of the instrument and of its subsystems. These design drivers are detailed in the subsequent sections. A whiskbroom scanning concept was selected (see section 2.2) in order to fulfill the high revisit time, requiring a large nominal swath of 687 km to be fast-scanned in less than 6 seconds, due to technological limitations in the along-track (ALT) dimension of the sensors. The ARA in the TIR bands (0.3K) at the reference temperature (300K) corresponds to 0.4% to 0.6% of the equivalent radiance (to be compared to 3.5% required in the solar bands) and can only be met with the implementation of a high frequency two-point on-board calibration scheme (see section 2.6). In both solar and thermal bands, the radiometric accuracy requires particular attention to stray light, which is controlled both by a careful optical design for ghost rejection (*cf.* section 2.3) and by the implementation of stray light correction in the data processing chain (*cf.* section 3.2). Time Delay Integration (TDI) is implemented on all bands to reach the high SNR (resp. low NEdT) and accommodate large scene signal dynamic. This operation is performed either by the Front End Electronics (FEE) or on-chip at detector level, depending on the bands (see section 2.5) and combined to pixel selection/deselection in relation with NSWIR and TIR detectors operability being lower than 100%. The spectral filtering and out-of-band rejection functions are ensured by a two-stage stripe filters design while tight spectral tolerancing is met by combination of optical design constraints (high telecentricity) and selection of first-class manufacturers.

Finally, the geometric performance (MTF, geolocation or spatial co-registration between the bands) demands very stringent pointing requirements on the scanner mechanism, presented in section 2.4), as well as a very good mechanical stability. A full-SiC optical telescope, benefiting from Airbus expertise and cumulated heritage on past space programs, and a careful attention brought to the thermal control keeps the thermo-elastic deformation

induced by the in-orbit environment to a level low enough to induce negligible impact on MTF compared to detector pixel and optical MTF.

Table 1. Collection of the LSTM instrument key requirements in the visible and near infrared (VNIR) and short wave infrared (SWIR) bands. This summary includes spectral performance (central wavelength and full width at half maximum (FWHM)), radiometric performance (minimum, reference and maximum radiances L_{min}, L_{ref} and L_{max} defining the required dynamic range, signal to noise ratio (SNR), absolute radiometric accuracy (ARA), relative spectral radiometric accuracy (RSRA), relative spatial radiometric accuracy (RXRA) and radiometric stability over time) and image quality specified by the modulation transfer function (MTF) of the L1b product at the Nyquist frequency of the Level 1c product, *i.e.* after re-sampling of the images on a 50 m regular grid.

	Units	VNIR0	VNIR1	VNIR2	VNIR3	SWIR1	SWIR2
Central wavelength	[µm]	0.490	0.665	0.865	0.945	1.380	1.610
FWHM	[µm]	0.065	0.030	0.020	0.020	0.030	0.090
L_{min}	[W/m^2/sr/µm]	11.70	3.31	0.95	0.51	0.06	0.4
L_{ref}	[W/m^2/sr/µm]	128.00	108.00	52.39	8.77	6.00	4.00
L_{max}	[W/m^2/sr/µm]	615.48	484.13	307.80	232.91	45.00	69.78
SNR @ L_{ref}	[-]	162	142	100	114	100	133
SNR @ L_{min}	[-]	10	10	5	10	5	10
ARA @ L_{ref}	[%]	3.5	3.5	3.5	3.5	3.5	3.5
RSRA @ L_{ref}	[%]	1.0	1.0	1.0	1.0	1.0	1.0
RXRA @ L_{ref}	[%]	0.5	0.5	0.5	0.5	0.5	0.5
Radiometric stability @L_{ref}	[%]	0.5	0.5	0.5	0.5	0.5	0.5
MTF @ L_{1c} Nyquist	[-]	0.2 - 0.3	0.2 - 0.3	0.2 - 0.3	0.2 - 0.3	0.2 - 0.3	0.2 - 0.3

2.2 Instrument overview

The selected concept of the LSTM instrument is illustrated on the functional diagram presented on Figure 3. The eleven spectral bands of the LSTM instrument are recorded on three separate focal planes: the visible detector (VIS) dedicated to the VNIR0, VNIR1 and VNIR2 bands, the short-wave infrared (SWIR) is used for VNIR3, SWIR1 and SWIR2, and the TIR detector images the five thermal bands. All three focal planes are accommodated in front of a single telescope. A pendulum scanner mechanism acquires a wide swath in the across-track direction, and allows for acquiring an on-board calibration black body source at every scan cycle as well as deep space acquisitions, both used for the calibration of thermal bands. Another calibration and shutter mechanism is able to insert a solar diffuser target in the optical path for the calibration of the solar channels in the exact same way as Sentinel-2 MSI calibration. A first dichroic beam splitter (DBS1, or VT-DBS for Visible-Thermal DBS) separates the optical paths of the TIR bands from the path of the solar bands, while a second DBS assembly, separates the VIS and SWIR path on their respective detectors. Spectral response function of the instrument is shaped via two layers of stripe filters. Each focal plane is enclosed in a specific assembly, providing the adequate thermal environment, *i.e.* ambient for VIS, passively cooled to 200 K for SWIR, and actively cooled at cryogenic temperature (65 K) for the TIR detector. The Instrument Control Unit (ICU) is the central piece of the instrument electronic control. It centralizes and distributes all Telemetry and Tele-commands (TM/TC) to the instrument units, handles the science data from the detector and interfaces with the spacecraft electronics and with the payload electronic modules, such as the Front-End Electronics (FEE) associated to each detector, the Mechanism Drive Electronics (MDE) or the Cryocooler Drive Electronics (CDE). The ICU controls the thermal regulation of the whole instrument via a large set of thermal sensors and heaters.

The LSTM instrument is embarked on a recurring platform, and its overall dimensions, mass power need and data transfer rate are sized to match its capability (*cf.* Table 3).

Table 2. Collection of the LSTM instrument key requirements in the thermal infrared (TIR) bands. The set of requirements is identical to the ones of VNIR-SWIR bands presented in Table 1, with an additional requirement about pseudo-noise. All radiometric performance are expressed in [K] in order to relate them directly to the measured brightness temperature. In particular the requirement about radiometric precision is expressed as a noise equivalent delta temperature (NEdT) rather than SNR.

	Units	TIR1	TIR2	TIR3	TIR4	TIR5
Central wavelength	[µm]	8.600	8.900	9.200	10.900	12.000
FWHM	[µm]	0.180	0.180	0.180	0.400	0.470
T_{min}	[K]	250	250	250	250	250
T_{ref}	[K]	300	300	300	300	300
T_{max}	[K]	460	460	460	460	460
NEdT @ T_{ref}	[K]	0.1	0.1	0.1	0.1	0.1
NEdT in $[T_{min} \ldots T_{max}]$	[K]	0.2	0.2	0.2	0.2	0.2
ARA @ T_{ref}	[K]	0.3	0.3	0.3	0.3	0.3
RSRA @ T_{ref}	[K]	0.1	0.1	0.1	0.1	0.1
RXRA @ T_{ref}	[K]	0.15	0.15	0.15	0.15	0.15
Radiometric stability @ T_{ref}	[K]	0.1	0.1	0.1	0.1	0.1
Pseudo-noise @ T_{ref}	[K]	0.4	0.4	0.4	0.4	0.4
MTF ALT @ L_{1c} Nyquist	[-]	0.2 - 0.3	0.2 - 0.3	0.2 - 0.3	0.2 - 0.3	0.2 - 0.3
MTF ACT @ L_{1c} Nyquist	[-]	0.15 - 0.3	0.15 - 0.3	0.15 - 0.3	0.15 - 0.3	0.15 - 0.3

Table 3. Instrument budgets

Size	$1550 \times 1705 \times 1420$ mm^3
Mass	<500 kg
Power	<450 W
Science data rate	126 Mbps (VIS), 168 Mbps (SWIR), 237 Mbps (TIR)

2.3 Optical design

The accommodation of three detectors dedicated to three spectral ranges in a single instrument relies on the LSTM original patented optical design (*cf.* Figure 4). The dual TMA is composed of five freeform mirrors in silicon-carbide (SiC) mounted on a single SiC baseplate. The primary mirror M1 is common to all spectral paths, and two sets of secondary and tertiary mirrors M2 and M3 compose the VNIRSWIR path on the one hand and the TIR path on the other hand. The number of refractive components is minimized so as to avoid ghosts and scattering stray light, thus no re-imaging optical systems are implemented. The entrance pupils (equivalent cicular diameter >200 mm in TIR and >130 mm in VNIRSWIR) are located at slightly different longitudinal positions in order to image their respective on-board calibration targets without any vignetting that would be detrimental to the radiometric accuracy. Area and shape of the pupil is optimized independently for TIR and VNIRSWIR optical paths in order to meet both SNR and MTF requirements. The focal length of each path is designed to provide the same pixel instantaneous field of view. The first stage of spectral filters is located in the intermediate focal plane beyond the DBS1. The second set of filters is located in front of the photosensitive surface of the detectors (see Figure 5). The accuracy and stability over the field of view of the spectral response is ensured by the very stringent telecentricity in both the intermediate and detector focal planes. This optical design pays particular attention to the control of stray light, and several features are implemented to reduce the amount of unwanted rays reaching the detectors. First, the telescope is integrated on a single monolithic baseplate. On one side the scan mirror, the calibration black body and the M1 are integrated. The beam is then directed through an aperture in the baseplate towards its other side, where the rest of the optical path, up to the
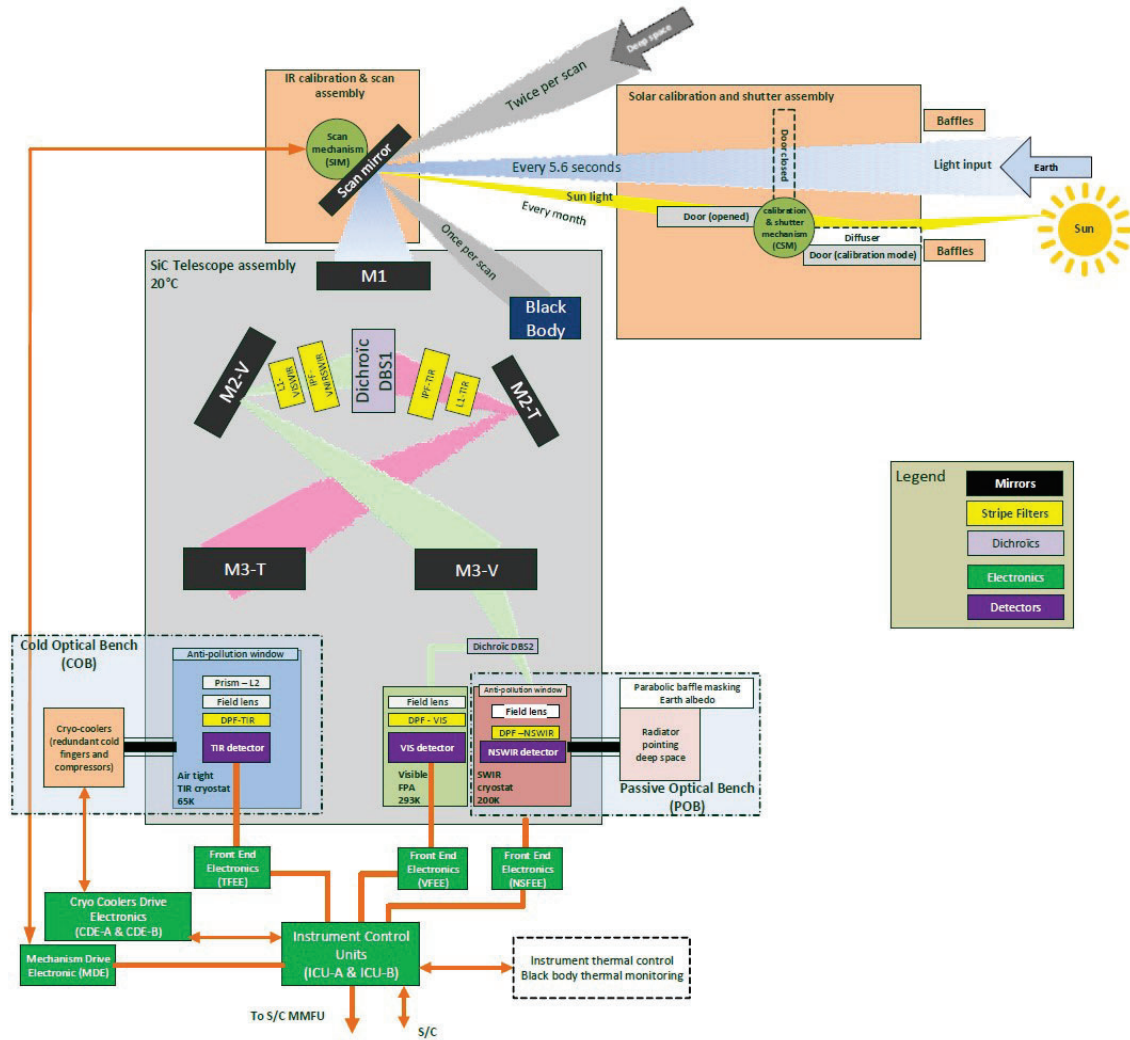
Figure 3. Functional diagram of the LSTM instrument

focal planes, is integrated. This physical separation between a front cavity and a rear cavity reduces the possible parasitic paths coming from direct entrance in the Earth observation view port. The double filtering stage also contributes to the stray light reduction by filtering out the spectral content out of the useful band, upstream of the focal plane assemblies. Several optical components are wedged in such way that most of the main ghost paths are geometrically rejected. The strong astigmatism introduced in the system by the wedged components is compensated by the introduction of a compensating prismatic lens in the Cold Optical Bench (COB).

2.4 Scanner mechanism

The LSTM scan mechanism (SCM) enables the instrument to successively observe the earth, the deep space port, and the on-board black body dedicated to the radiometric calibration of the thermal bands. The scan sequence, pictured on Figure 6, consists in the observation of the earth (+/- 29° LoS angles centered on Nadir, corresponding to 687 km of nominal swath on-ground) with a constant velocity, followed by an acceleration to successively acquire the deep space port, stop on the black body, and quickly return to its initial position while
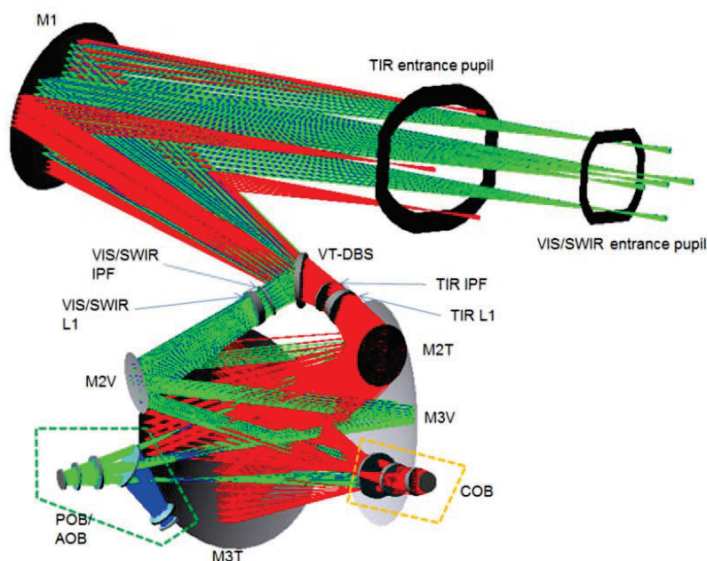
Figure 4. Optical design of the LSTM instrument - *Patented* - France, Patent demand 2005561 deposited 26/05/2020*
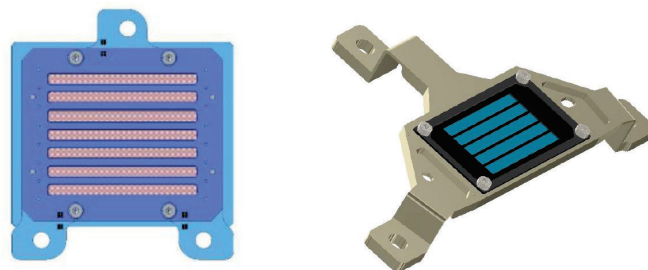
Figure 5. Stripe filters of the VNIRSWIR path at the intermediate focal plane (left) (courtesy of OBJ and IOF) and of the TIR path at the detector focal plane (right) (courtesy of the University of Oxford)

acquiring the deep space port a second time. The short repeat cycle duration (5.7s) ensures that successive swaths are acquired without any gap in the data, and with sufficient overlap to allow efficient image reconstruction.

Several key performance of the instrument are directly linked to the scan mechanism performances. For instance, the Spatial Sampling Distance (SSD) in the ACT direction is defined by the LoS angular displacement during the frame time (254 µs), meaning that the drift of the pointing performance from one frame to the next leads to an instability of the SSD, and a relative pointing error occurring between TDI stages (see section 2.5) will affect the MTF through the effect of TDI desynchronization. Similarly, the knowledge of the scanner position provided by the mechanism encoder must be very good in order to guarantee the image geolocation with a sufficient accuracy. These requirements demands for a mechanism with very stable motion velocity, low wobbling and high performance encoder. To fulfill these challenging requirements, AIRBUS selected the state-of-the-art DSM (Dual Swing Mechanism) stepper mechanism from IASI-NG that benefits from exhaustive qualification campaigns.[4]

2.5 Detection chain

As mentioned in section 2.2, three separate detectors are used to cover the LSTM spectral range. The VIS detector covers the first half of the solar channels (VNIR0, VNIR1 and VNIR2 from 0.490µm to 0.865µm), the SWIR detector is dedicated to the second half (VNIR3, SWIR1 and SWIR2 from 0.945µm to 1.610 µm) and the
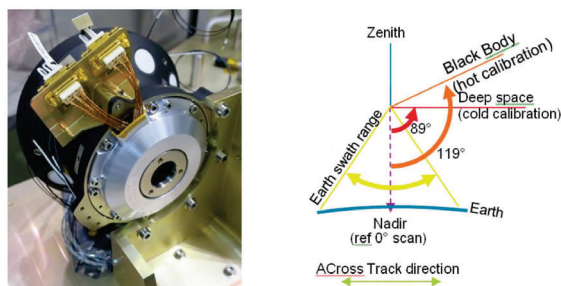
Figure 6. LSTM scan mechanism (left) and scanning sequence (right)

TIR detector to the five thermal bands (TIR1 to TIR5 from 8.6 µm to 12 µm). Each detector has its dedicated driving FEE, which are all piloted by the ICU.

The three detectors have many important features in common despite their different suppliers, technologies and implementations. Each spectral band is associated to a CMOS stripe detector, with the long edge oriented along the ALT direction, acquiring one row of the swath at a time, corresponding to a given position of the scan. Their location at the focal planes of a common telescope, and the fact that they image the same ALT swath ensure that the acquired swath of each spectral channel overlaps, which ensures a native very good spatial co-registration between the spectral bands.

The acquisition mode of all bands is based on time delay integration, in order to optimize the SNR, although the number of TDI stages depends on the specific radiometric constraints of each band. The TDI acquisition concept, illustrated on the top part of Figure 7, is based on the fact that the imaged scenes is translated over the detector plane by the scanning motion. Hence, to improve the signal acquired on a given target point on ground, the same point is acquired from several pixels along the scan direction (*i.e.* the ACT direction) and the signal from all the acquired pixels is added up. This imposes that the frame time (254 µs) is perfectly synchronized with the time the scanner needs to sweep a distance equal to the pixel pitch. As described in section 3.1, a desynchronized acquisition between TDI stages contributes to the MTF performance, similary to scan motion smearing during integration period.

In the visible chain, detector pixels operability is 100% and all rows are therefore used for TDI. On the SWIR and TIR bands on the other hand, it is expected that a number of pixels are defective (*i.e.* cannot meet the SNR requirements) and have to be left unused. For this reason, the number of rows of the detector is larger than the number of TDI stages that are actually used. The bottom part of Figure 7 displays an example (illustrative only) where 4 TDI stages are used on 9-pixel wide window. The pixels in green on this figure represent non-defective pixels that are used to integrate the signal, while the orange pixels are deselected and their signal is not considered. A Look Up Table (LUT) is characterized before launch and used for the pixel deselection.

2.5.1 VIS detection chain

The VIS detector is a CMOS image sensor based on front-illuminated Si detection layer, featuring very low dark current when operated at ambient temperature. The VIS detector is integrated in the ambient optical bench (AOB) without any need for cooling. The photosensitive area is composed of two rows of 1200 pixels (15 µm pixel pitch) in the ALT direction in VNIR0 and VNIR1 and four rows in VNIR2. The TDI summation is performed at FEE level.

2.5.2 SWIR detection chain

The SWIR detector is composed of a n/p HgCdTe (or MCT) detection layer, hybridized on a Read Out Integration Circuit (ROIC), based on CMOS technology.[5] It features four photodiode sub-arrays, two of them are binned to increase the signal in VNIR3 and the two others are associated to SWIR1 and SWIR2. Each photodiode comprises 12 rows of 1200 pixels. The TDI process can be applied to all 12 rows but a selection/deselection process is implemented to allow discarding defective pixels. Up to 2 pixels per column can be deselected without affecting the SNR performance. Contrary to the other two detectors, the TDI summation is performed on-chip. The SWIR detector is operated at 200 K, and is integrated in the Passive Optical Bench (POB).
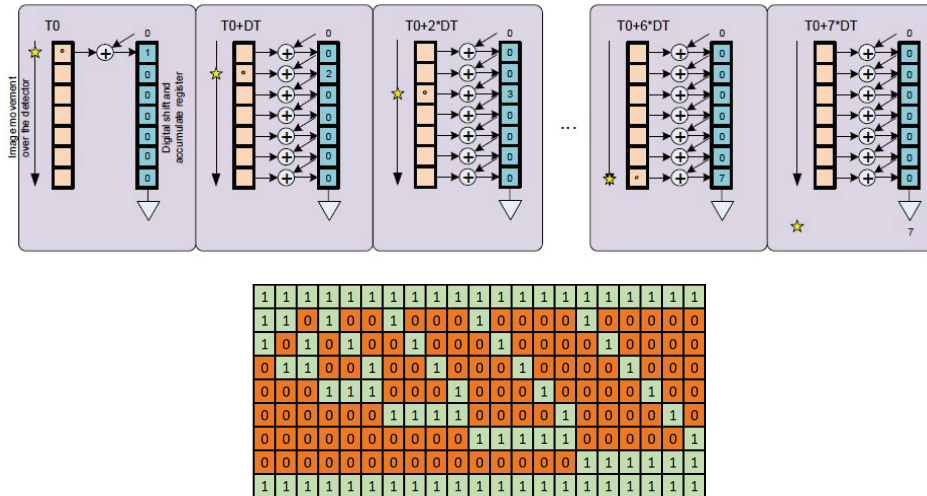
Figure 7. Principle of Time Delay Integration and example of pixels deselection with 4 TDI stages among a window width of 9 pixels
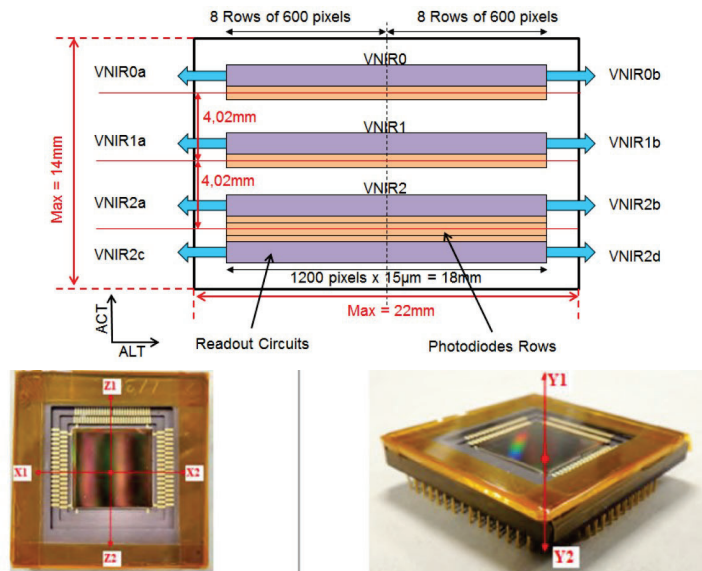
Figure 8. Schematics of the VIS detector (top), picture of the detector package (bottom) (courtesy of ADS - ISAE)

2.5.3 TIR detection chain

The TIR detector relies on a new generation of LWIR and VLWIR technology able to provide large ALT dimensions and high data rate. Two low dark current p/n MCT photodiode arrays hybridized on large ROIC based on CMOS process compose the TIR retina, covering the bands TIR1, TIR2, TIR3 (first PV array) and TIR-4 and TIR-5 (second PV array), as illustrated on Figure 10. The coverage of the ALT swath of the instrument is ensured by 1088 pixels. Each PV subarrays has 32 pixels in the ACT direction in which a readout window is selected in which the number of defective pixels is minimized. This, feature, coupled with pixel deselection prior to TDI performed by the FEE, allows maximizing the available SNR while maintaining an operable rate of pixels of 100%. A tradeoff on MCT absorber thickness is necessary to maximize the internal detection efficiency, favoured by a thicker absorbing layer, and the detector MTF which benefits from a thinner layer.[6] The TIR
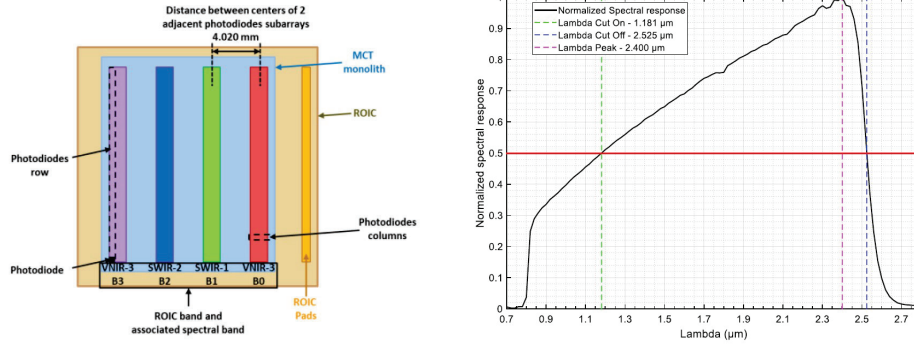
Figure 9. Schematics of the SWIR detector (left) and typical spectral response (right), (courtesy of Lynred)

detector is operated at 65 K in order to guarantee low dark current performance and is therefore enclosed in an actively cooled cryostat (cold optical bench, *cf.* section 2.8).
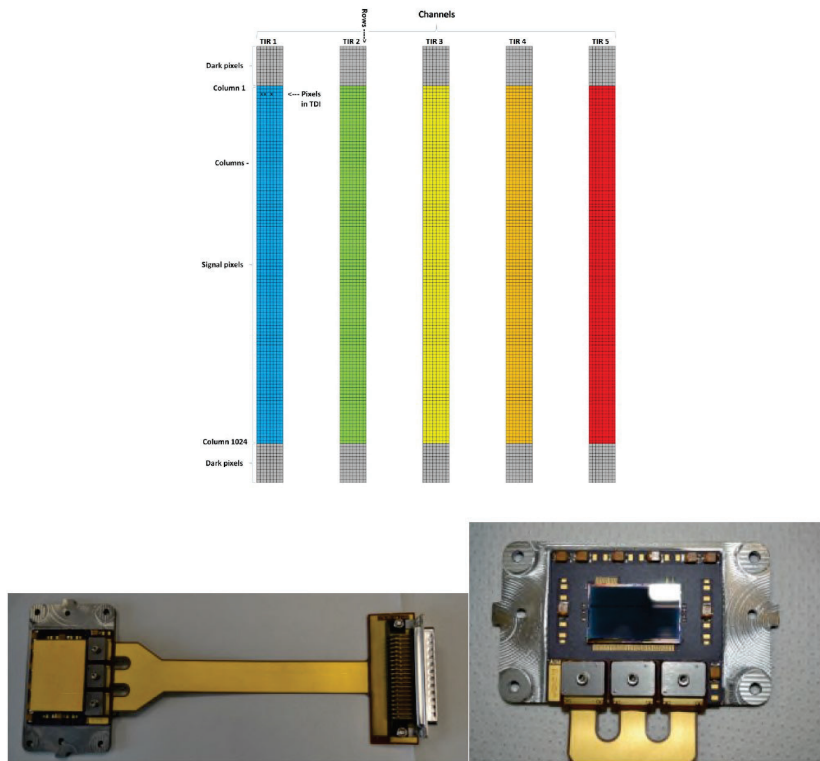
Figure 10. Schematics of the TIR detector layout (top), pictures of the pre-development TIR detector (bottom) (courtesy of AIM)

2.6 On-board radiometric calibration

The thermal infrared on-board calibration source (OBCS) consists of a surface black body with unregulated temperature slowly varying around 290K. Its large emissive surface covers the full pupil, and allows for the simultaneous radiometric calibration of the complete detector area. An accurate monitoring of the black body

temperature at all time, coupled with a very good spatial uniformity over the OBCS surface are key to guarantee the quality of the radiometric calibration performed at every scan repeat cycle. The acquisition of the deep space port completes the TIR calibration scheme by providing a reference dark acquisition at every cycle.

The solar channels calibration is not sensitive to the variations of the thermal environment and only requires the monitoring of long term drifts. A large solar diffuser is mounted on the instrument aperture door and allows, as the OBCS in the thermal bands, for a full pupil calibration. Acquisitions of the sun diffuser, introduced in the instrument aperture to be addressed by the scanner mirror, are expected to be performed on a monthly basis. This calibration sequence of the Sun channels is identical to the calibration performed on the AIRBUS built Sentinel-2 MSI instrument using recurrent diffuser.[7]

All calibration targets are integrated in positions addressable by the scanning mirror in its nominal operation motion. The optical chain from the calibration target up to the detector is therefore identical to the optical path followed by the Earth radiation minimizing by design calibration errors and avoiding the use of additional dedicated optics and mechanism.

2.7 Mechanical design

The high mechanical stability required to meet the instrument pointing performance and to ensure the optical quality relies on a full SiC telecope assembly relying on AIRBUS heritage on previous programs such as Gaia, MSI, ATLID for ESA and export programs. As illustrated on Figure 11, the double cavity telescope (*cf.* section 2.3) is entirely integrated and aligned on a single SiC baseplate. The scan mechanism and the primary mirror, the two optical elements composing the front cavity, are integrated on one side of the baseplate. The secondary and tertiary mirrors of the solar and thermal bands, the first dichroic assembly (including the first filtering stage), and the three focal plane assemblies are integrated on the other face of the baseplate. The full SiC design guarantees a very high mechanical stability by minimizing the thermo-elastic deformation of the assembly along the orbit. Three optical heads of star tracker units are also mounted on the telescope structure, allowing improved performance of the satellite pointing performance.

The SiC telescope assembly is interfaced on the Instrument External Structure (IES) thanks to four CFRP (Carbon-Fiber-Reinforced Polymers) bipods. This structure accommodates the different electronic units (CDE, MDE and ICU), the Calibration and Shutter Mechanism as well as the calibration blackbody. The IES also supports all thermal radiators and the secondary hardware such as the heat pipes, electrical harness, connectors, optical baffles and MLI (Multi-Layer Insulator). The second important function of the IES is to interface the whole instrument onto the platform. The S- and K- band antennas, as well as the gyros, although platform components, are directly accommodated on the IES.

2.8 Thermal design

The control of the thermal environment is of particular importance for an infrared instrument, for two main reasons.

First, every surface at a given temperature emits a thermal flux, which depends on its temperature and emissivity. Therefore, each component of the LSTM instrument contributes to the thermal background flux, which is, by nature, in the spectral range detected by the TIR detector. The thermal background must therefore be of limited amplitude, in order to leave sufficient dynamic range to the detector for the detection of the useful flux, and at the same time, remain extremely stable in order to maintain a good correspondence between the measured flux and the Earth brightness temperature, *i.e.* to maintain a good absolute radiometric accuracy. The stability horizon is reduced by the presence of the on-board calibration source allowing for a radiometric calibration of the TIR band every 5.7 seconds. Within this time window however, the temperature variation cannot be corrected.

The second driving feature for the thermal control is the operating temperature of the detectors. The low dark current performance that is necessary to ensure the high SNR (resp. low NEdT) is provided at 200K for the SWIR detector and 65K for the TIR detector.

These constraints translate in the need for a distinct thermal control for the telescope assembly (including scan mechanism and ambient optical bench), the passive optical bench and the cold optical bench.
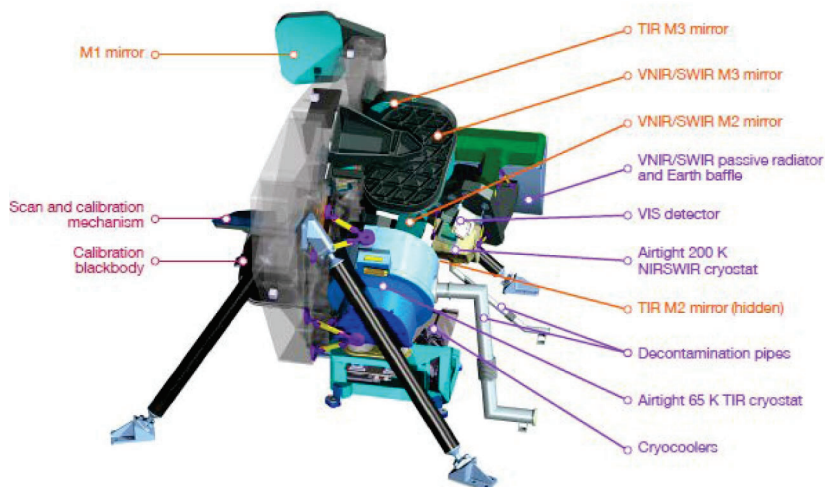
Figure 11. LSTM mechanical design overview

Heating lines on the telescope baseplate, scan mechanism are dedicated to maintain these elements around 20°. The high conductive thermal coupling of the monomaterial SiC to SiC interfaces between the mirrors and the baseplate ensures that the optical surfaces are kept stable without additional heater control system.

The SWIR detector is enclosed in the Passive Optical Bench (POB) and is passively cooled down to 200 K thanks to a dedicated radiator, left unexposed to any earth or sun exposure over the orbit and combined to a parabolic baffle directing the Earth view out of the baffle surface in order to limit the incident heat flux. The detector package is linked to the radiator thanks to a thermal strap. The optical components inside the POB (*cf.* Figure 12) are naturally operated at cold temperatures. The stripe filters positioned very close in front of the detector are kept at the same temperature through conductive coupling, and the field lens and window temperature are around 215K and 250K respectively, through radiative transfer mainly.

The cryogenic temperature of the thermal detector (65 K) asks for an active cooling system. The TIR focal plane assembly is enclosed in a cryostat and connected to a pair of cryocoolers accommodated on the instrument external structure through dedicated cold fingers assemblies. The cryostat keeps the TIR optics (stripe filters, field lens and prism) at cold temperature, and a dedicated internal cold optical baffle limits the thermal background close to the detector surface.

3. KEY PERFORMANCE

3.1 MTF performance

Static and dynamic contributors drive the instrument MTF. The first category includes contributions fixed by the hardware design and integration, and are essentially the telescope WaveFront Error (WFE) and the detector intrinsic MTF. The dynamic contributors are related to effects induced by LoS motion. Image smearing results from the displacement of the scene in front of the detector during the integration time. Part of the smearing is generated by the nominal scan motion during integration and part is generated by perturbations of the nominal scan motion due to the earth rotation, the satellite velocity which are two deterministic elements, and pointing instabilities from scanning mechanism, micro-vibrations induced by cryocoolers. The combination of the earth rotation, satellite velocity and scanning motion is largely compensated by aligning the detector with an in-plane angle such that its axes are aligned with the average combined displacement vector. The pointing instabilities on the other hand were anlaysed and lead to stringent requirement on the SCM accuracy and on the micro-vibrations control.
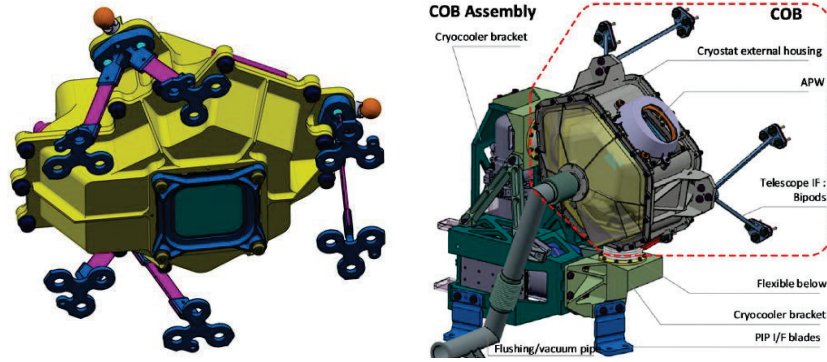
Figure 12. Passive Optical Bench (left) and Cold Optical Bench (COB) overviews

The instrument MTF performance simulated at the beginning of the project are presented on Figure 13. The MTF in ACT and ALT direction at the Nyquist frequency after resampling at 50m equivalent frequency, averaged over the field of view, and in worst case orbital position, is presented for each band against the position in the swath with large variation between the Nadir position (swath center) and the edge where the requirement applies.
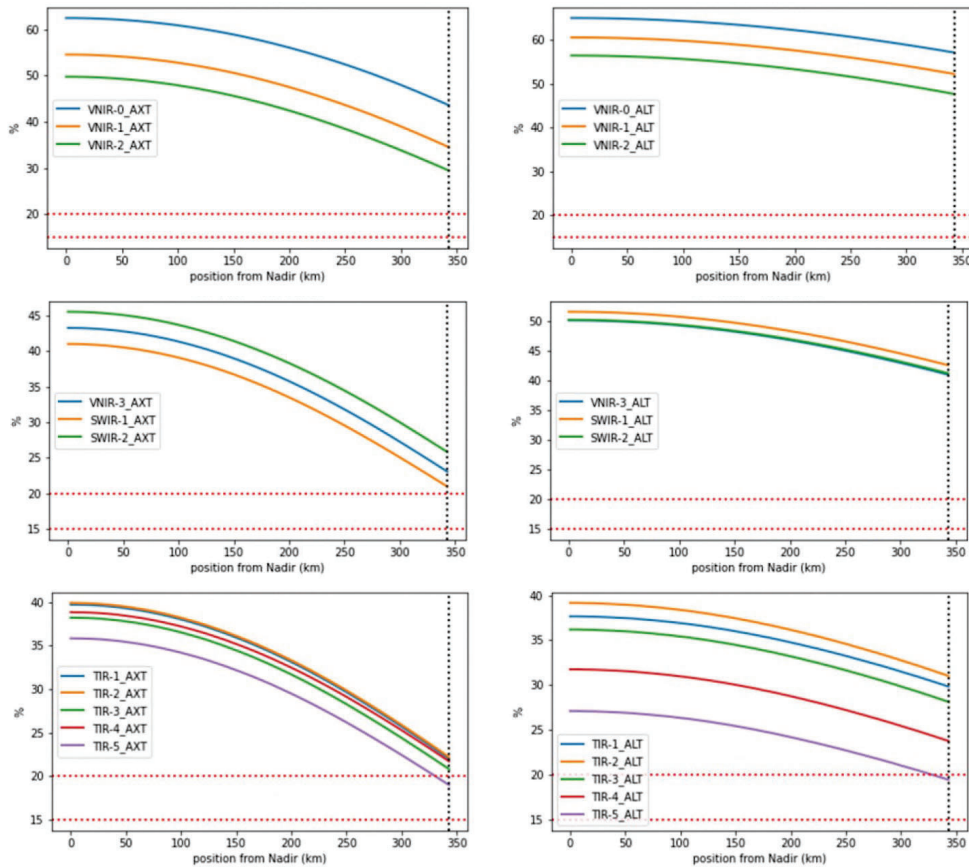
Figure 13. MTF performance plotted against the position in the swath

3.2 Radiometric performance

As discussed in section 2.1, the main radiometric performance are the signal-to-noise ratio in solar channels (expressed as noise equivalent delta temperature in thermal bands), and the absolute radiometric accuracy, ensuring the required precision and accuracy of the retrieved scientific products such as LST and ET. The SNR (resp. NEdT) is specified for reference scenarios of Top Of Atmosphere (TOA) radiance spectra in the visible to SWIR bands, and for reference brightness temperatures in the thermal bands (see Figure 14). For performance analysis, the brightness temperature is converted to radiance levels assuming a perfect black body radiation thanks to Planck's black body radiation law.
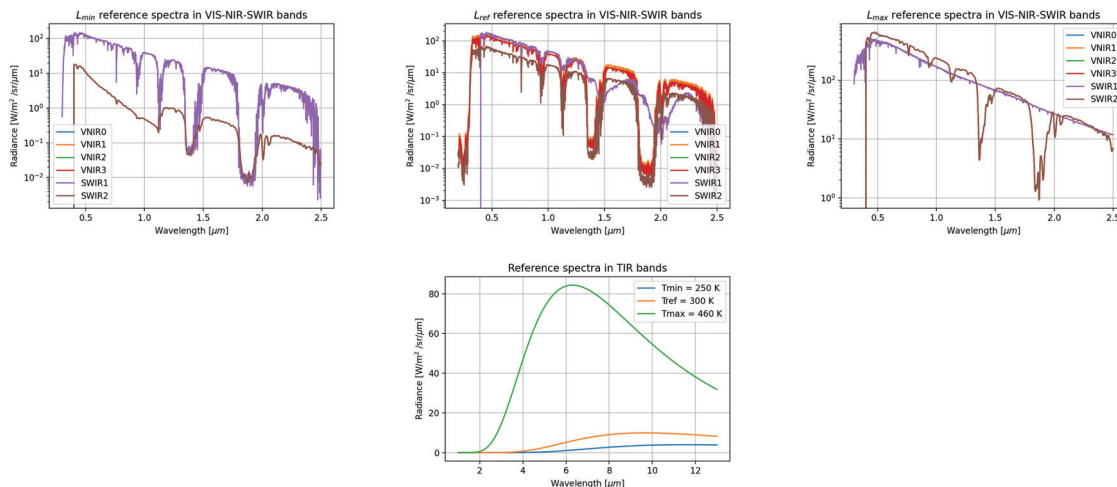
Figure 14. Radiance reference spectra in solar channels (top) and in thermal bands (bottom)

$$L_{\mathrm{BB}}\left(\lambda, T\right) = \frac{2hc^2}{\lambda^5} \frac{1}{\exp\left(\frac{hc}{\lambda k_{\mathrm{B}} T}\right) - 1} \tag{1}$$

Large entrance pupils, optimized optical coatings, removal of refractive components and low dark current detectors are part of the design features implemented to maximize the available flux as well as minimizing the noise. Another particular attention is paid in the thermal bands to the level and stability of the thermal background flux incident on the detector, for instance by a careful optical design and baffling of the COB. The additional gain brought by the TDI scheme described above allows the instrument to fulfill the targeted performance, as shown on Figure 15.

The absolute radiometric accuracy quantifies the *trueness* of the scientific radiometric product provided by the instrument. The main challenges associated to meeting this performance are on the one hand the stability of the radiometric calibration in the thermal bands, and on the other hand stray light control in all spectral bands.

The stray light control is partly ensured by the optical design, as discussed in section 2.3. However, the analysis based on a detailed stray light modeling of the instrument shows that the stray light levels generated by pure diffraction and scattering exceeds the acceptable levels which are necessary to maintain the targeted ARA even with systematic ghost-busting optical design optimization. In particular, the ARA is specified on a theoretical worst case non-uniform scene scenario consisting in a half-space at a reference bright radiance (resp. brightness temperature) and the other half space at a reference low radiance (resp. brightness temperature), as illustrated on Figure 16. In such a scene, the ARA performance must be guaranteed down to a minimum distance of 5 SSD from the sharp transition from bright to dark levels.

The instrument stray light analysis reveals that the parasitic signal is too high by a factor of 4 to 10 in the bands VNIR0 to VNIR2, 24 to 30 in VNIR3, 10 to 12 in both SWIR bands and finally 20 to 30 in the thermal
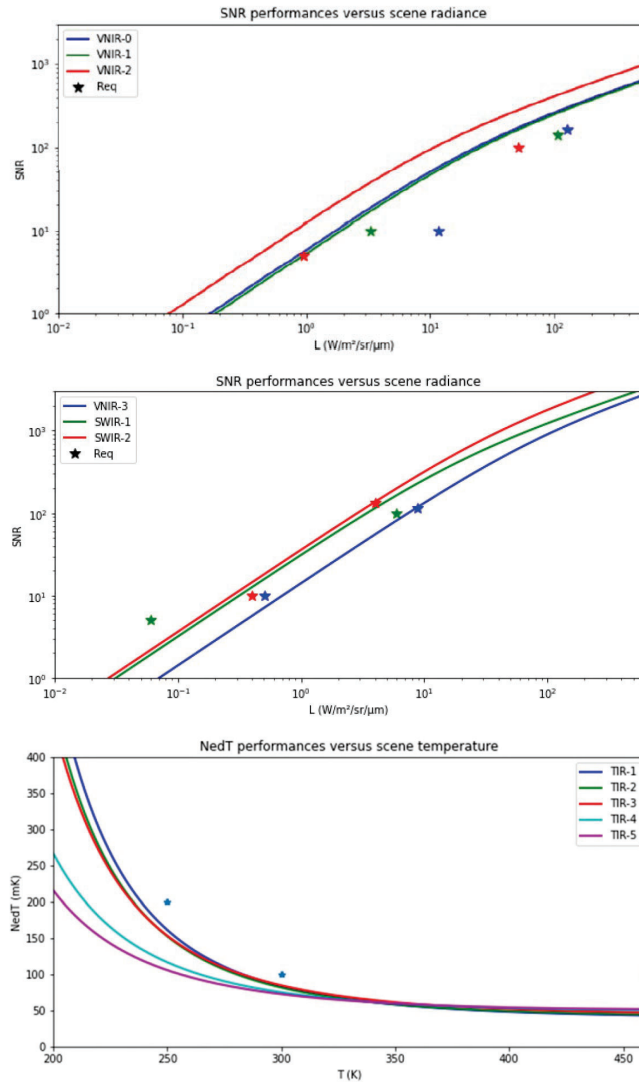
Figure 15.   SNR performance compared to specified level, against TOA radiance (VNIR-SWIR) and NEdT against brightness temperature (TIR)

bands. For this reason a stray light correction scheme is added as part of the data processing. The correction algorithm is based on the evaluation of the stray light signal from the acquired scene and the instrument PSF calibrated on-ground, which is then subtracted from the acquired scene. This type of algorithm is successfully implemented on several other ESA missions.[8–10]

4. TECHNOLOGY READINESS STATUS

One hard programmatic requirement of the LSTM mission is the demonstration of a sufficient technology readiness level (TRL-6) of the critical elements is demonstrated by the system Preliminary Design Review (PDR). The critical elements include the three detectors as well as the filters and the dichroic beam splitters.

For instance, dedicated pre-development activities have been carried on for the most critical components, in order to anticipate the design and development activities and demonstrate the performance thanks to detailed

Figure 16. Typical non-uniform scene used as reference scenario for the evaluation of absolute radiometric accuracy

breadboarding activities. These activities were performed during early phases of the program and has validated the selection of the critical suppliers. This phase was for instance the opportunity to demonstrate the feasibility of the optical coatings needed to meet the filtering and beam splitting requirements and the associated tolerance.

The main scope of the technology demonstration in the current development phase consists in demonstrating the resistance of the hardware against the storage, launch and in-orbit environments, and the stability of its performance within these environments. In order to do so, an early testing approach on specific development models has been implemented and are currently on-going.

For the optics, the set of tests is mainly separated between the optical coating resistance, which requires the tested unit to be representative for the substrate and the applied optical coating, and the assembly, *i.e.* the optics in their mechanical mounts. The first aims at demonstrating the optical performance, such as spectral stability or optical transmission, and the latter is used to demonstrate the mechanical stability, and the absence of deformation due to thermal or mechanical loads. A similar multi-level verification strategy is applied to the detector, as some tests are performed at ROIC level only (to test the resistance of the read-out electronics), at FPA level, *i.e.* with the detection layer already hybridized on the ROIC and on the full detector package.

5. CONCLUSION

We have presented an overview of the Copernicus LSTM instrument, designed by AIRBUS to meet the mission overall objective to provide global measurement of the land surface temperature and evapotranspiration with an unprecedented combination of high spatial and temporal resolution. The translation of this objective into the payload main requirements is detailed, as well as the main design drivers, leading to the presentation of the technological choices that have been implemented. The status of the key performance of the instrument is presented, showing that the LSTM instrument design is fully compatible with the scientific goals. Finally, we have presented the strategy of anticipated development aiming at validating the technology readiness in early stage of the project.

ACKNOWLEDGMENTS

REFERENCES

[1] "Copernicus High Spatio-Temporal Resolution Land Surface Temperature Mission: Mission Requirements Document." ESA, 2021 https://www.esa.int/Applications/Observing_the_Earth/Copernicus/Copernicus_Sentinel_Expansion_missions.

[2] Lagouarde, J.-P., Bach, M., Sobrino, J., Boulet, G., Briottet, X., Cherchali, S., Coudert, B., Dadou, I., Dedieu, G., Gamet, P., Hagolle, O., Jacob, F., Nerry, F., Olioso, A., Ottle, C., Roujean, J.-L., and Fargant, G., "The mistigri thermal infrared project: Scientific objectives and mission specifications," *International Journal of Remote Sensing* **34**, 3437 (05 2013).

[3] Grandell, J. and Stuhlmann, R., "Limitations to a geostationary infrared sounder due to diffraction: The meteosat third generation infrared sounder (mtg irs)," *Journal of Atmospheric and Oceanic Technology* **24**(10), 1740 – 1749 (2007).

[4] Calvel, B., Faure, F., and Penquer, A., "IASI-NG development status," in [*International Conference on Space Optics — ICSO 2020*], Cugny, B., Sodnik, Z., and Karafolas, N., eds., **11852**, 118523Y, International Society for Optics and Photonics, SPIE (2021).

[5] Jamin, N., Salvetti, F., Baud, L., Berthoz, J., Martineau, L., and Chorier, P., "New developments of mutlilinear and multispectral infrared sensors for space applications at Lynred," in [*10th International Symposium - Optro2022*], (2022).

[6] Hanna, S., Bauer, A., Bitterlich, H., Eich, D., Finck, M., Figgemeier, H., Gross, W., Mahlein, K., and Wegmann, A., "Space application requirement breakdown and sensor concept implementation for mct-based lwir and vlwir 2d high-performance focal plane detector arrays at aim," *Journal of Electronic Materials* **49**, 6946–6956 (11 2020).

[7] Martimort, P., Fernandez, V., Kirschner, V., Isola, C., and Meygret, A., "Sentinel-2 multispectral imager (msi) and calibration/validation," in [*2012 IEEE International Geoscience and Remote Sensing Symposium*], 6999–7002 (2012).

[8] Tol, P., Kempen, T., Hees, R., Krijger, M., Cadot, S., Snel, R., Persijn, S., Aben, I., and Hoogeveen, R., "Characterization and correction of stray light in tropomi-swir," *Atmospheric Measurement Techniques* **11**, 4493–4507 (07 2018).

[9] Abdon, S., Armand, D., Laurent, F., Barillot, M., D'Ottavi, A., Coppo, P., Luca, E. D., Gabrieli, R., Bouvet, M., François, M., and Taccola, M., "Digital correction of residual straylight in FLEX images," in [*International Conference on Space Optics — ICSO 2018*], Sodnik, Z., Karafolas, N., and Cugny, B., eds., **11180**, 1662 – 1675, International Society for Optics and Photonics, SPIE (2019).

[10] Babic, L., Manzillo, P. F., Esposito, M., Loots, E., Ludewig, A., Kleipool, Q., Grabarnik, S., Bernard, F., and Courrèges-Lacoste, G. B., "A stray light correction analysis framework for the calibration of Sentinel-4/UVN," in [*International Conference on Space Optics — ICSO 2020*], Cugny, B., Sodnik, Z., and Karafolas, N., eds., **11852**, 1351 – 1364, International Society for Optics and Photonics, SPIE (2021).